IEEE Access
Multidisciplinary | Rapid Review | Open Access Journal

Received 22 January 2024, accepted 23 February 2024, date of publication 18 March 2024, date of current version 1 April 2024.

Digital Object Identifier 10.1109/ACCESS.2024.3378743

RESEARCH ARTICLE

Advancing Satellite Network Performance: Network Analysis for Federated Satellite Systems

SIMONE SCROCCIOLANI, VINCENZO MESSINA, RAMÓN MARÍA GARCÍA ALARCIA, JASPAR SINDERMANN, AND ALESSANDRO GOLKAR
Department of Aerospace and Geodesy, Technische Universität München, 85521 Ottobrunn, Germany
Corresponding author: Alessandro Golkar (golkar@tum.de)

ABSTRACT An increasing number of satellite constellations being deployed in orbit fosters the introduction of a more efficient paradigm of distributed, interconnected orbital assets to ensure better resource exploitation in orbit. This paper aims to illustrate through quantitative modeling the effects of satellites on board available resources and inter-satellite telecommunication hypotheses on the overall operations of a federated satellite system network. Key research questions addressed by this work include the performance quantification of a one hundred CubeSats federated satellite system network in terms of network response and data volume exchanged under several onboard resource constraints. The applicability of a federated satellite system to a time-critical disaster response monitoring scenario has also been verified to assess the practical implementation of such a paradigm in reduced inter-satellite communicability conditions. A distributed simulator based on the IEEE 1516-2010 standard is employed to obtain the federated satellite system network topology according to the individual satellite operations to analyze the network performances, exploiting an approach based on the network's adjacency matrix. Despite reduced communicability, which limits the average inter-satellite link to an 8 bps time-averaged goodput due to poor onboard resources availability, the federated satellite system proves to be an auto-sufficient and decentralized paradigm, capable of responding to a time-critical scenario such as a rapid mapping request after a natural disaster in under 6 hours. As a result, this work provides the foundation for more detailed development of a federate satellite network, compliant with current radiofrequency regulations.

INDEX TERMS Aerospace simulation, communication networks, global earth observation system of systems, satellite communication, small satellite.

I. INTRODUCTION

Nowadays the requirements for temporal and spatial resolution in the field of Earth observation are becoming more stringent. Increased coverage and higher temporal and spatial resolution requirements require the shifting the current space mission design paradigm from a single monolithic satellite mission to distributed and heterogeneous satellite system concepts [1]. Satellite constellations, one instance of distributed satellite systems, has recently became popular due to the emergence of mega-constellations leveraging on the increased availability of cost-effective small spacecraft, and the decrease of launch costs enabled by reusable launchers. These paradigm changes enabled increased adoption of constellation architectures by the commercial space industry. Examples of new constellations include those deployed by Planet (optical imaging) [2], Starlink (telecommunications) [3], and ICEYE Ltd. (radar imaging) [4]. The services provided by such commercial constellations range respectively from visible, infrared, and microwave imaging in Earth Observation, to broadband and narrowband connectivity in telecommunications. Federated satellite system (FSS) is a relatively new instance of distributed satellite system concept enabling the development of

The associate editor coordinating the review of this manuscript and approving it for publication was Rosario Pecora.

a heterogeneous satellite network, facilitating opportunistic collaboration of spacecraft pursuing a common goal. In a FSS, satellites can dynamically join a federation composed of several other satellites sharing resources (as providers) or requesting services (as clients) in a negotiation, market-based environment [5]. A possible field of application for FSS is represented by disaster response monitoring. This is due to the extremely stringent requirements in terms of temporal availability (usually a sub-daily target revisit time coupled with nearly global coverage) required for rapid mapping tasks for post-disaster situational awareness. In addition, the rising of extreme natural events caused by climate change requires a more integrated approach to post-disaster rapid mapping. Different remote sensing instruments can observe diverse features of the Earth and sensor data fusion is fundamental to provide additional insights into the processes affecting Earth surface with respect to previous data products of the satellite missions. To achieve nearly simultaneous and multispectral target acquisitions, greater integration and cooperation between existing orbital assets (such as in a FSS) need to be accomplished [6]. In order to allow such cooperation, multiple challenges have been identified in [7].

1) Heterogeneous radio hardware: Despite being grouped in a relatively small number of frequency bands, telecommunication hardware, such as antennas, is optimized for limited frequency channels and correlated with satellite size and cost, yielding compatibility issues at the physical layer.
2) Security issues: Exposing a federate to unauthenticated inter-satellite communications can pose security threats such as lack of confidentiality, integrity, and availability.
3) Link disruption: Due to satellite networks' high mobility, the network topology changes continuously. In the case of FSS, this issue is exacerbated by the unforeseeable on-demand nature of the federation, which is dynamically created to respond to a task, according to the federation participants' needs and resources.
4) Asymmetric links: Due to hardware heterogeneity yielding different radio transmission powers, different channel throughput characterize two-way inter-satellite links.
5) Large delays: Communicating over thousands of kilometers imposes latency periods which must be tolerated by the protocol stack and error correction scheme chosen for the FSS network.

These challenges have been addressed in a number of works available in the literature. For instance, [8] proposes the pairing of a FSS with a telecommunication mega constellation such as Telesat to overcome network disruption and highlights the FSS capability of augmenting downlink data volume for a federation of Earth observation satellites. In addition, [9] proposes a solution to link disruption by exploiting a proactive protocol stack capable of autonomous network discovery, specifically tailored for FSS requirements. The exploitation of a Public Key Infrastructure to address FSS security is illustrated in [10], allowing for federate authentication and malicious federation user identification. Reference [11] analyzes the applicability of wireless network standards to heterogeneous satellite networks. In addition, methods for data rate control on asymmetric links, specialized for asymmetry tolerant protocols such as Saratoga are investigated in [12]. To progress from the proposed networking and protocols solutions to a proven product for effective deployment in a future FSS, a simulation environment is needed. Previous works concentrated on different solutions to develop a link-oriented FSS simulator. The most popular network simulators for aerospace applications are NS2/3, OMNeT++ and Qualnet [9]. However, most of the approaches utilize a preprocessing of orbital and satellite attitude data from astrodynamics-specific software (such as AGI STK) to be fed to the network simulator [13]. Additional modules for enhanced physical layer modeling fidelity have been introduced in such network simulators, as in [14]. However, this approach does not permit a full closed-loop simulation, in which satellites' attitudes and operations can be influenced by satellite links and network operations. Such a problem has been solved by running simultaneously AGI STK and the network simulator stopping the execution at each time step at the price of a slow simulation rate [15]. A more advanced, fully integrated solution is presented in [16], in which the authors integrated the possibility of modeling custom satellites in a network simulation environment. Such a simulator, however, does not foresee any integration of hardware in the loop modules. Software-defined radios (SDR) are regarded as a powerful tool to verify with an effective on-the-air, hardware-produced data exchange the performance of novel protocol stacks [17]. For this reason, a hardware-in-the-loop capable simulator, with the additional possibility of network simulator extendability (such as OMNeT++), is needed to conduct a fully realistic verification of the previously proposed protocols. Such a simulator would be capable of assessing the impact of operational and communication hypotheses on the FSS network performance. In fact, most of the solutions and protocols previously presented are also tested in real-case scenarios; however, the rules to engage an inter-satellite communication are based on preliminary link budget analysis in which the maximum ISL range results in the only constraint to communication [8]. In addition, [18] highlights the lack of proper network connectivity estimation in practical applications such as algorithms for Earth observation sensor webs optimal task scheduling. As a result, the practical feasibility of such optimal algorithms is severely underestimated.

The research objective of the present paper focuses on the development of a HIL-capable, model-based FSS simulator as a tool to model inter-satellite links between federates, superimposing the effects of FSS participation to the regular operations of a satellite, authorizing the satellite participation to the FSS solely when allowed by sufficient onboard

resources. Specifically, the present paper unfolds to address two precise research sub-objectives:

1) Analyzing the influence of operational and resource constraints on inter-satellite communication of a FSS network.
2) Assessing the impact of network connectivity on a time-critical FSS autonomous task scheduling scenario, such as rapid mapping for disaster response monitoring.

The remainder of this paper is structured as follows: Sec. II presents the methods that allow the production of the results. The results are presented and analyzed in Sec. III. Sec. IV summarizes the work contained in the present paper, answers to the research objectives previously stated, and discusses possible extensions to the present work.

II. METHODOLOGY

This section presents the methods employed to assess FSS network performances and the real-case scenario adopted to test the FSS network. An overview of the overall methodology followed during the present paper is presented in Fig. 1. The FSS simulator outputs the signal-to-noise ratio (SNR) of each ISL. This information is then treated by exploiting graph theory to run additional post-processing simulations to characterize network performances. The same approach is then followed for the disaster response monitoring use case. Specifically, Sec. II-A shows the development of a FSS-compatible distributed simulator with potential HIL capabilities for FSS protocol testing. The hypotheses regarding the FSS architecture are presented in Sec. II-B. The simulator is then employed as a workhorse to generate the data used in Sec. II-C to infer network performance.

A. SIMULATOR DEVELOPMENT

To capture the heterogeneity of a federated satellite system, great interoperability among different simulators is needed. This is due to the need to connect multiple simulators or FlatSats via radio hardware in the loop for communication protocol end-to-end testing at a later protocol verification and validation stage. As a result, to model a system of systems and interoperate different simulators, six main challenges are identified and reported by [19]:

1) Technical: common information exchange mechanism.
2) Syntactic: common data syntax or structure.
3) Semantic: common data semantics or vocabulary.
4) Pragmatic: common context of data workflow or usage.
5) Dynamic: two-way interactive information exchange.
6) Conceptual: mutually compatible conceptual model.

These challenges are approached with the framework provided by distributed simulation standards such as IEEE 1516-2010, also known as High Level Architecture (HLA) [20]. The co-simulation of the same scenario potentially connecting multiple satellite simulators and FlatSats requires in fact a secure data transmission between the simulators allowing for remote operations and avoiding the need to disclose excessive knowledge regarding the simulators, possibly being owned by multiple competitive and suspicious organizations. Furthermore, distributed simulation standards such as the High Level Architecture also allow to distribute the computational load of the simulator among multiple machines, allowing for more detailed simulations while maintaining an efficient and standardized data exchange. This HLA features properties of particular interest for the development of a subsystem-level simulator of a federated satellite system, characterized by modularity and ease of expansion. The general nature of the standard allows the HLA to be hardware-agnostic, allowing dynamic federate joining, thus opening the possibility of using even in-orbit satellites as simulation nodes. The most fundamental component of a simulation federation, as prescribed by the HLA standard, is the run-time infrastructure (RTI). The RTI is a software middleware permitting to interface multiple simulators and allowing data exchange for the concurrent co-simulation of the same mission scenario via a publish and subscribe mechanism. Several RTIs implementations are currently available, and previous work demonstrates CERTI open-access nature and high performance with large payload data sizes to be the optimal choice for this application [21]. An object-oriented programming approach is applied to the modeling and simulation of each satellite participating in the simulation. Four C++ simulation models propagate the overall state of the satellite in terms of orbital position, attitude, electrical power, and telecommunication subsystem. Each simulation federate composing the distributed simulation federation runs multiple satellites to split the computational load among several machines. CERTI HIL capabilities are demonstrated in [22], however the HIL integration with satellite hardware has been verified connecting to the simulation a radio receiver via SPI, exploiting a Raspberry Pi 3B board as a hardware bridging CERTI and the radio module. An overview of the hardware setup on which the distributed simulation architecture is run is presented in Table 1.

TABLE 1. Simulator hardware setup components.

Component	Quantity	Function
Ethernet cabling cat. 6 F/UTP	6	Simulation network connection
Power Supplies	9	Hardware power delivery
NETGEAR GS116 switch	1	Simulation network connection
NRF24L01 radio module	2	Radio modules
Raspberry Pi 4B	5	Simulator computing pool
Raspberry Pi 3B	1	Radio receiver-HLA interface
Arduino UNO R3	1	Radio message generator
Input/output peripherals	2	Simulation control

B. FSS SATELLITE TYPE CONFIGURATION

The standard satellite type participating in the simulated FSS is a 6U CubeSat. The adoption of the CubeSat standard is fostered since it represents a useful worst-case scenario for onboard resources. The platform is modeled with two additional deployable solar panels. The satellite bus is complemented by two payloads: an RGB electro-optical imager and a GPU for AI applications. The concept of operations

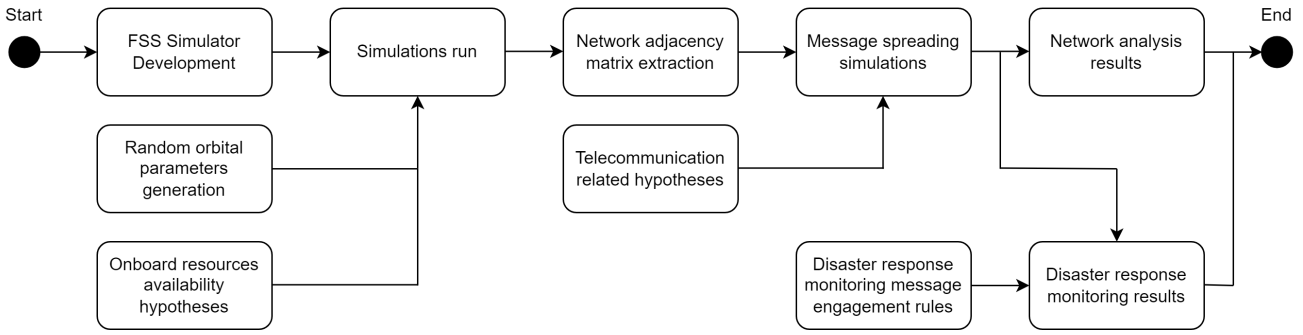

FIGURE 1. Overview of the methods workflow employed to generate the results.

TABLE 2. Inter-satellite link budget parameters.

Parameters	Value	Unit
Max. TX power	1	W
Antenna max. gain	1	dBi
TX Losses	2	dB
Carrier Frequency	437	MHz
Path Attenuation	0.5	dB
Modulation	FSK	-
FEC scheme	Convolutional (K=7, R=0.5) or RS(255,223)	-
Bandwidth	9600	Hz
RX Losses	2	dB
RX Sensitivity	-121	dBm
RX Noise Figure	0.9	dB
RX temperature	481.5	K
Required E_B/N_0	2.50 or 9.75	dB
Data rate	9600	bps

assumes that inter-satellite link transmissions are possible whenever excess power with respect to battery charging is produced by the solar panels; signal reception is always possible. This assumption allows for a seamless superposition of the FSS network operations over the nominal satellite operations. The inter-satellite communication function is granted by a UHF telecommunication terminal model based on an EnduroSat UHF Transceiver II and an EnduroSat UHF Antenna III. Useful hardware and communication parameters for the calculation of a link budget are presented in Table 2. The choice of a UHF omnidirectional antenna allows for inter-satellite communication without extremely restricting pointing requirements or reorientations. Additionally, the choice of a frequency inside the UHF amateur band (430 - 440 MHz) is coherent with a common choice for many SmallSats, due to the flexibility of not having to procure a commercial radio license and the overcrowded situation of the commercial UHF band. Accordingly with the FSSCat mission [23], considering the adoption of a Reed Solomon RS(255,223) FEC scheme in a best-case scenario for communications, an inter-satellite link range of around 1200 km can be achieved [8].

C. SIMULATOR OUTPUT POST-PROCESSING

In order to proceed with the network analysis, a one hundred CubeSat federation has been simulated. The simulator's output consists of the inter-satellite link E_b/N_0 for all the possible inter-satellite connections. This output can be rearranged in matrix form, resulting in the adjacency matrix of a weighted and directed graph in which every matrix column identifies one transmitting satellite and one hundred receivers. The network analysis is based on the assessment of the channel goodput, the effective data rate achievable without considering low-level protocol headers. This paper assumes that the FSS communication is based on a variation of the protocol stack presented in [9]. The protocol is therefore supposed to be based on Saratoga, BATMAN, and AX.25 respectively at the transport, network, and data link layers. The adoption of AX.25, despite a reduced maximum frame size, is due to CubeSat hardware compatibility. The addition of a FEC scheme further reduces the goodput. The overall maximum attainable goodput for both the encoding schemes presented in Table 2 is presented in Table 3. The information provided by the E_b/N_0 to goodput conversion allows rewriting the adjacency matrix substituting the signal strength with the quantity of useful payload data that can be transmitted. To effectively compare and determine the FEC scheme which ensures the highest overall quantity of data transmitted, the goodput and the number of inter-satellite contacts can be weighted in time for each inter-satellite connection as shown in (1).

$$\overline{G}_{ij} = \frac{1}{N_{sim}} \sum_{k=1}^{N_{sim}} A_{ij}(t_k) \tag{1}$$

where $\overline{G}_{ij}$ represents the time-averaged goodput in bps between satellites i and j, N_{sim} is the total number of simulated time steps, and $A_{ij}(t_k)$ is the goodput-converted adjacency matrix element corresponding to the inter-satellite connection i,j associated to the t_k time step. Analyzing the spectrum of time-averaged goodput produced by all the possible inter-satellite links allows to deduce which FEC scheme is capable of optimizing the overall exchanged data volume. To understand the dynamics of message spreading related to the communication and resources hypotheses, a set of manipulations of the adjacency matrix has been used. The list of those adjacency matrix reworks is presented as it follows:

TABLE 3. Maximum goodput FEC scheme comparison (channel throughput 9600 bps).

FEC Scheme	Min. E_b/N_0	Max. Goodput
Reed-Solomon RS(255,223)	9.75 dB	5710 bps
Convolutional (K=7, R=0.5)	2.50 dB	3260 bps

1) Temporal Stacking: This operation allows to exclude from the adjacency matrix the short-lived contacts. Exploiting a moving stack of N adjacency matrices (associated to N-1 precedent time steps, with a first in first out philosophy), only permanent connections throughout the whole temporal stack are maintained in the adjacency matrix (as shown in (2), where $A_{ij}^{[k]}$ represents the adjacency matrix element associated to satellites i,j referring to the simulation time step k).

$$A_{ij}^{[k]} = \begin{cases} 0 & \prod_{n=0}^{N} A_{ij}^{[k-n]} = 0 \\ \dfrac{\sum_{n=0}^{N} A_{ij}^{[k-n]}}{N} & \prod_{n=0}^{N} A_{ij}^{[k-n]} \neq 0 \end{cases} \tag{2}$$

2) Symmetrization: This operation forces a structural symmetry to the adjacency matrix. The location of nonzero elements is therefore symmetric (as shown in (3) where $A^{[k]}|_{>0}$ represents the binary adjacency matrix (converting each nonzero element to the value of 1) associated with time instant k.). Such an operation allows the imposition of half-duplex constraints for communication.

$$A_{ij}^{[k]} = \begin{cases} 0 & A_{ij}^{[k]}|_{>0} \neq A_{ji}^{[k]}|_{>0} \\ A_{ij}^{[k]} & A_{ij}^{[k]}|_{>0} = A_{ji}^{[k]}|_{>0} \end{cases} \tag{3}$$

After the adjacency matrix A has been manipulated via the aforementioned operations, message propagation through the network is managed via recursive multiplication of a message reception binary state vector and the time-stamped adjacency matrices. The propagated state vector after k time steps can be written as in (4).

$$\vec{x}^{[k]} = \left(\left(\prod_{n=0}^{k-1} \left(I + A^{[k-n]}|_{>0} \right) \right) \cdot \vec{x}^{[0]} \right) \Big|_{>0} \tag{4}$$

It must be noted that a delay operation on the message propagation state vector x can be applied to model processing delays between the reception of the message and the first available retransmission. The performance metrics used to assess network capabilities are mainly two:

1) Time to spread (TTS_x): This metric identifies the time needed to spread a message to the $x\%$ of the FSS participants.
2) Time to next contact (TNC_x): This metric identifies the time needed to spread a message to the next FSS node after the $x\%$ of the network has been already reached.

The relation among the two performance indexes can be expressed as in (5), in which y represents the percentual increase driven by a novel single satellite contacted in the network.

$$TNC_x = TTS_x - TTS_{x-y} \tag{5}$$

The shortcoming of the aforementioned performance metrics resides in their initial state dependency. Therefore, to get a complete spectrum of results the initial message state must be perturbed to vary the initial satellite spreading the message. This approach, despite being accurate, is computationally demanding, requiring a Monte Carlo-based approach. Therefore, additional communication metrics directly linked to the adjacency matrix structure have been investigated. Specifically, three measures of centrality and communicability have been analyzed. The first metric is the degree centrality of each node composing the network. The degree of a node represents the number of edges involving that node. In the case of a directed network, the degree is additionally split in in-degree and out-degree to correctly capture the directionality of the edges insisting on the node [24]. In an undirected graph, the degree of each node i can be expressed as in (6).

$$D_i = \sum_{k=1}^{N} a_{ik} a_{ki} = \left(A^2 \right)_{ii} \tag{6}$$

Despite being extremely straightforward, this metric takes into account only a local picture of the network surrounding the node [24]. A more general approach considers not only the edges departing from a node but the walks of every possible length k between two nodes i, j. If the counting of walks is included and longer walks influence is scaled according to the factorial of their respective length $k!$, the Estrada communicability is retrieved as in (7) [24].

$$E_i = \sum_{j=1}^{N} \sum_{n=1}^{N} \phi_n(i) \phi_n(j) e^{\lambda_n} = \sum_{j=1}^{N} \sum_{k=1}^{\infty} \frac{\left(A^k \right)_{ij}}{k!} \tag{7}$$

where $\phi_n(i)$ represents the i-th element of the n-th orthonormal eigenvector associated with the n-th eigenvalue λ_n of the adjacency matrix of the network A [25]. Summing over the rows generates a communicability concentrated on the transmission capabilities of each node. However, both the metrics proposed represent the connections of a static network, in which the edges remain the same over time. A dynamic network introduces a time-dependent evolution that interferes with the network communicability, generating an asymmetry [26]. A message from node i to j can only follow a path if that path is unfolding in the correct direction according to the time passing. This asymmetry can be captured by employing a dynamical version of Katz centrality (a centrality measure based on the combinatorics of walks) (8).

$$K_i = \sum_{j=1}^{N} \left((I - \alpha A)^{-1} \right)_{ij} \tag{8}$$

where α is a scaling parameter that decrements the importance of walks of length l with respect to walks of length $l-1$ and must be smaller than the inverse of the spectral radius of A [26]. The dynamic approach consists of multiplying all the time-stamped centrality measures (characterized by a different adjacency matrix) in a single product (9), to be then summed along the rows to retrieve a single centrality measure that already takes into account the network evolution [26].

$$K_i^D = \sum_{j=1}^{N} \prod_{k=1}^{N_{sim}} \left(\left(I - \alpha A^{[k]} \right)^{-1} \right)_{ij} \tag{9}$$

The choice of α is crucial to tune the importance given to the different walk lengths. In fact, minimal values of α tend to collapse K^D to a shifted aggregate of degree centralities, whereas, for values of α close to their upper bound (equal to the inverse of the spectral radius), only an instantaneous snapshot of the network is effectively considered for calculations [26]. For this reason, during the analysis, an $\alpha = 0.005$ revealed to remain within the boundary set by the spectral radius for each of the simulations tested and maintain the correlation coefficient between Katz centrality and aggregate degree centrality below 0.5. These adjacency matrix-related quantities are subsequently evaluated against the overall network TTS_{100} (for the remainder of this paper shortened in TTS) under a series of hypotheses greatly modifying network topology to assess an eventual empirical relation existence.

III. RESULTS

A. SIMULATOR VALIDATION

The first set of results to be presented regards a validation of the simulator. The simulator output is compared with the theoretical results of a link budget between the satellites presented in Table 6. The satellites are characterized by polar, coplanar, and concentric keplerian orbits, with an initial true anomaly separation of 10 degrees. In addition, the satellite antennas are supposed to be perfectly omnidirectional. All the other parameters are unchanged with respect to the ones presented in Table 2.

This configuration yields a repetitive contact pattern with a maximum E_b/N_0 equal to 8.47 dB. The contact is repeated circa every 16 hours. This theoretical evidence is confirmed by the output of the simulator as presented in Fig.3.

B. NETWORK ANALYSIS

A set of seven different simulations has been analyzed. The simulations hypotheses affect both on-board resources availability and telecommunication properties are the following:

1) Perfect pointing (hypothesis ID: PP): every link is supposed to happen with a perfect alignment of the satellite antennas.
2) Full power (hypothesis ID: FP): the satellites can transmit with the maximum RF power along the whole orbit.
3) Federation participants (hypothesis ID: RX): X satellites on randomly generated orbits compose the network.
4) Simplex - half duplex (hypotheses IDs: SX, HD): identifies the communication setting required for the protocol to work efficiently.
5) Processing delay (Hypothesis ID: DX): upon the reception of a message, the satellite requires an onboard processing delay of X seconds before being capable of transmitting the message.
6) Link persistence (Hypothesis ID: CX): to consider a message exchange between two satellites to be successful, the link must persist in time for a minimum of X seconds.

The hypotheses characterizing each simulation are illustrated by Table 7. The choice of 100 satellites in the federation is motivated by the actual order of magnitude of satellite constellations achieved by constellations of similar form factors (e.g. Planet Labs Inc. Doves). In addition, 30 seconds are assumed to be sufficient to provide federates the network next hop information, as well as Doppler effect correction [27].

The results regarding the time-averaged goodput and TTS results spectrum for each one of the simulation are presented in Fig. 4 and Fig. 5 respectively.

The first remark regards the superiority of a softer encoding approach such as RS(255,223) with respect to the convolutional code. This is due to the sufficient robustness provided by the former encoding scheme with respect to the extremely reduced effective data rate of the latter. On-board resource scarcity greatly affects the time-averaged goodput, especially simulations 1, 2, and 3 (which differ from one another by pointing or on-board power availability) show a sharp decrease of goodput, which is less evident for telecommunication-related hypotheses (simulations 4 to 7). However, it must be noted that the mean time-averaged goodput, even for the almost ideal conditions of simulation 1, is reduced to 295 bps (with respect to 5710 bps, the highest goodput the channel can provide out of a throughput of 9600 bps). Such a difference confirms that despite the best available conditions in terms of onboard resources are strongly limited by a federation random orbital configuration. Moreover, it highlights a structural telecommunication shortcoming of the satellite federation with respect to satellite telecommunication constellations, whose orbital design is carefully crafted to ensure high data throughput.

This result confirms the necessity for such a UHF-radio-based federation network with the aforementioned hypotheses to optimize data exchange. However, telecommunication-related hypotheses still have a significant impact on TTS. The average time to spread a single-frame message to the whole network ranges from 4 minutes (simulation 1) up to 11 hours (simulation 7). A significant increase in TTS can be observed between simulations 5 and 6, in which the minimum contact duration to consider a contact

successful is increased from 30 to 100 seconds. Increasing the minimum contact time required, especially in a non-pre-designed orbital configuration of the FSS, hits the hard limit of satellite orbit dynamics, as well as a higher power consumption to sustain. In conclusion, the goodput and TTS behaviors are related to the different natures of the two families of hypotheses. The onboard resource scarcity mostly affects the quality of the links (such as contact duration), whereas the telecommunication-related hypotheses impact network topology directly.

Simulation 5 is regarded as the most realistic for a low data rate use case, and therefore, it has been analyzed in more detail. The spectrum of TTS result for simulation 5 shown in Fig. 5 is exposed in Fig. 6. The result highlights the nonlinear dynamics of message spreading. The whole envelope of the results shows the high dependability of the message-spreading dynamic with respect to a perturbation of the satellite initially seeded with the message, however, some considerations can be drawn when observing the time average of all the simulations. A message spreading throughout a FSS behaves similarly to how a virus spreads during an epidemic. In fact, the message initially spreads throughout the network following exponential growth. Subsequently, the message spreads with a linear behavior until the last, poorly communicative satellites are reached, slowing down the completion of the spreading process. Moreover, Fig. 7 shows, exploiting the TNC metric (both maximum and average values), how both the initial and final parts of the spreading process are also the ones undermining spreading robustness and repeatability.

Two possible operations can enhance the network response:

1) Multiseeding shortens the TTS reducing the effect of the initial communication bottleneck by seeding the same message from the ground segment to multiple federation participants simultaneously.
2) A spreading cutoff shortens the TTS reducing the effect of the final communication bottleneck, excluding the least communicative satellites from message reception.

Fig. 8 shows the beneficial reduction effect of a multiseeding strategy over TTS. Moreover, for multiseeding operations with more than 3 satellites, TTS is also more robust to exaggerated maximum values, which remain limited to 5 hours. The addition of a spreading cutoff is instead capable of reducing TTS, up to 30%, excluding the 5% least communicative satellites. The importance of the spreading cutoff is confirmed by the sensitivity analysis on the network TTS presented in Fig. 9. The effect of a perturbation on five relevant simulation network parameters on the TTS have been analyzed. The chosen parameters are the spreading cutoff percentage, the number of satellites in the federation, the link margin applied to the E_b/N_0 calculation, the onboard processing time before retransmission, and the minimum contact time required to consider a data exchange successful. The nominal and perturbed parameters for the sensitivity analysis are presented in Table 8.

As shown in Fig. 9, the spreading cutoff has the greatest sensitivity impact on the TTS, which, on average, is lowered from 5.27 hours to 4.02 hours with a cutoff on the 5% least communicative satellites.

The results on the three communicability metrics are presented in Fig. 10, Fig. 11, and Fig. 12 respectively. In addition to the seven simulations presented in Table 7, an additional data set from a different federation has been added for generality purposes. The novel federation is specialized in Earth observation, and instead of a random orbit generation, it is composed of satellites in polar and Sun Synchronous orbits (mainly concentrated around a local time of the ascending node equal to LTAN = 10.30 AM).

In the following paragraphs, it is possible to empirically verify that the TTS is, on average, governed by the least communicative satellite in the network. Katz centrality is computed as a single number per satellite, regardless of time, whereas Degree centrality and Estrada communicability produce time-dependent measurements, which are therefore time-averaged to provide a single quantity per satellite per simulation. After this harmonization, the least communicative satellite is extracted for each one of the three metrics.

The results highlight how all the metrics tend to have a moderate negative correlation between the minimum node communicability/centrality and the TTS. Estrada communicability reaches a flat condition for minimum node communicability slightly below 1, not capturing information relevant to the network state. This is due to the incapacity of centrality and communicability measures to quantify correctly poor communicators [28]. In addition, despite having a lower minimum time averaged degree centrality, the Earth Observation specialized network is producing a relatively short TTS. This difference is possibly motivated by the incapacity of such a metric to link the temporal evolution of the network paths. Coherently with a more complete theoretical model, Katz's dynamic centrality captures the dynamics of the Earth Observation network coherently with the results curve provided by the random satellites network. This might suggest that Katz's dynamic centrality may be a suitable parameter to estimate the average TTS of a satellite network. However, many practical limitations remain:

- Poor robustness: a limited number of seven simulations composing the results curve
- Poor adaptability: simulations must be run with the same time step and the same simulation duration for all the different networks to output comparable results

In conclusion, despite the presented shortcomings, Katz dynamic centrality may be a suitable predictor for the network TTS with a reduced computational load; however, a more extensive validation data set shall be tested.

C. DISASTER RESPONSE MONITORING CASE STUDY

To assess the practical feasibility of a FSS in a time-critical scenario such as disaster response monitoring, the following scenario is proposed:

"The FSS shall autonomously schedule to observe a target area of interest (AOI) affected by a natural disaster within a certain time frame and wavelength range. The scheduling algorithm shall be based on a decentralized auction method in order to test the effective inter-satellite interaction capability."

The approach followed in this paper relies on the onboard self-evaluation of a reward function J by each FSS participant. In order to balance the representation needs of both the data product (image) quality and onboard resource availability, the weighted reward function presented in (10) is introduced.

$$J = w_{IMG} \cdot J_{IMG} + w_{Battery} \cdot J_{Battery} + w_{ADCS} \cdot J_{ADCS} \quad (10)$$

For which J_{IMG} represents the data product quality, $J_{Battery}$ and J_{ADCS} are respectively associated with the battery's state of charge, and the slew angle needed to capture the target area into the imaging swath with respect to a nominal nadir-pointing attitude. A possible instance of the data product quality term J_{IMG} for optical imaging systems is presented in (11):

$$w_{IMG} \cdot J_{IMG} = w_{Cloud} \cdot J_{Cloud} + w_{Sun} \cdot J_{Sun} \quad (11)$$

The data product quality contribution J_{IMG} can be in fact decomposed in a term evaluating the Sun elevation on the target J_{Sun} and another term J_{Cloud} accounting for the cloud coverage over the target. The specific implementation of each reward function term is presented in (12).

$$\begin{aligned} J_{Sun} &= \frac{\vec{r}_{ET}}{||\vec{r}_{ET}||} \cdot \frac{\vec{r}_{TSUN}}{||\vec{r}_{TSUN}||} \\ J_{Cloud} &= 1 - \frac{C_C}{100} \\ J_{Battery} &= \begin{cases} 1 & \text{if } C > 1.1\, C_{safe} \\ 0 & \text{if } C \leq 1.1\, C_{safe} \end{cases} \\ J_{ADCS} &= 1 - \frac{acos\left(\frac{\vec{r}_{SE}}{||\vec{r}_{SE}||} \cdot \frac{\vec{r}_{ST}}{||\vec{r}_{ST}||}\right)}{\pi} \end{aligned} \quad (12)$$

Fig. 2 reports the convention adopted for the vectors $\vec{r}_{ET}$, $\vec{r}_{TSUN}$, $\vec{r}_{ST}$, and $\vec{r}_{SE}$; whereas C_C represents the cloud coverage percentage over the target and C the battery charge state. A safeguard threshold needs to be implemented in order to avoid the possibility that satellites characterized by extremely favorable onboard resources and extremely poor image quality are tasked with the observation. Two strategies have been implemented:

- J terms minimum thresholding. Each of the four subterms composing the reward function J_{Sun}, J_{Cloud}, $J_{Battery}$, J_{ADCS} are bounded to a [0,1] interval. However, the lower limit of this interval can be modified to avoid the aforementioned issue. The limits selection is shown in Table 4.
- w weights selection. In order to prioritize image quality over onboard resources weights have been assigned to each reward function term. Moreover, the greatest importance has been assigned to the cloud coverage measure, capable of seriously compromising the imaging campaign. The ADCS weight has been assigned a higher priority rather than the battery one since it is an indicator of deviation from the satellite's nominal operations. Moreover the energy cost of a single image acquisition is very limited. The weights can be consulted in Table 4.

TABLE 4. Reward function weights and minimum safeguards.

Reward function term	Min. J_x	Weight w_x
J_{Sun}	0.087	0.3
J_{Clouds}	0.7	0.4
$J_{Battery}$	1	0.1
J_{ADCS}	0.5	0.2

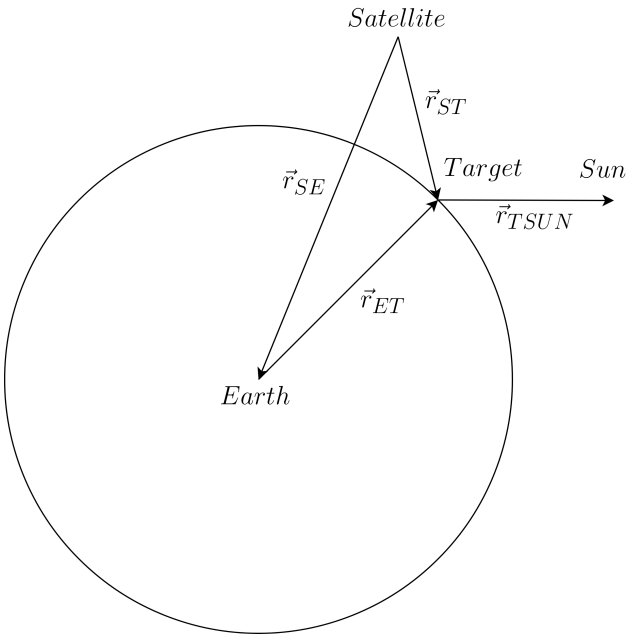

FIGURE 2. Conventions adopted for $\vec{r}_{ET}$, $\vec{r}_{TSUN}$, $\vec{r}_{ST}$, and $\vec{r}_{SE}$ in a 2D simplified representation of the geometry of the problem.

The concept of operations associated with autonomous task scheduling is inspired by [29]. Four different mission phases are identified in order to let the network negotiate which satellite will observe the target. The phases are listed as it follows in chronological order:

1) Task seeding: the observation task is transmitted from the federation's ground segment to one or more satellites.
2) Task spreading: the task spreads among the FSS participants via ISLs. Following the reception, the reward function is computed onboard.
3) Reward function bidding: The federation participants bid their reward function value following a gossiping protocol, progressively eliminating the least fit satellites.
4) Target observation: The fittest satellite proceeds to the target observation.

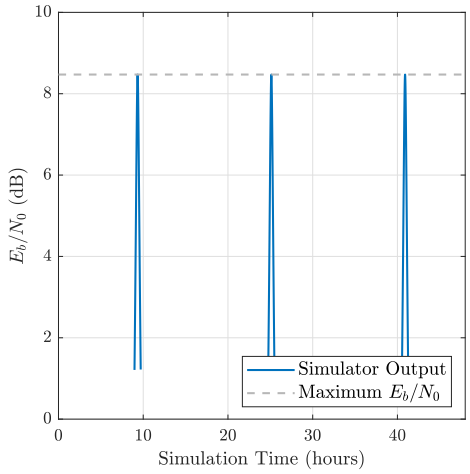

FIGURE 3. Contact pattern resulting from the simulator validation case test run. The contact (peaking at the minimum inter-satellite distance) is repeated every 16 hours circa.

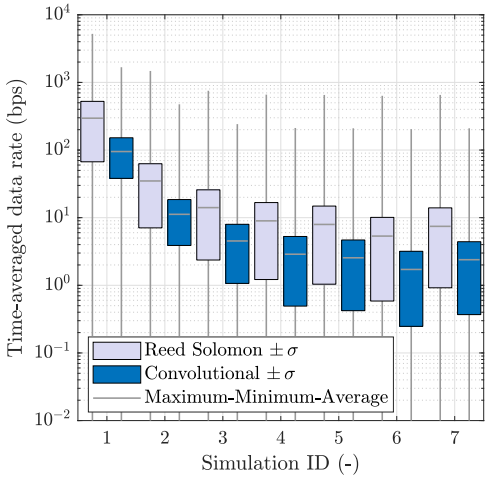

FIGURE 4. Time averaged goodput results spectrum for the various simulation profiles illustrated in Table 7. Maximum, minimum, standard deviation, and average values are presented for each simulation and coding scheme.

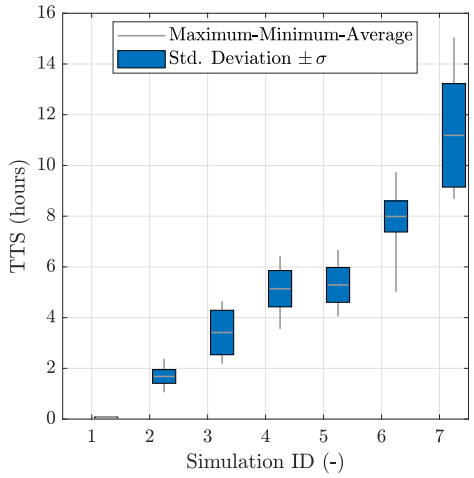

FIGURE 5. Single-frame message time to spread (TTS) results spectrum for the various simulation profiles illustrated in Table 7. Maximum, minimum, standard deviation, and average values are presented for each simulation. The results have been obtained via a Monte Carlo approach varying the satellite originally aware of the message at the beginning of the simulation.

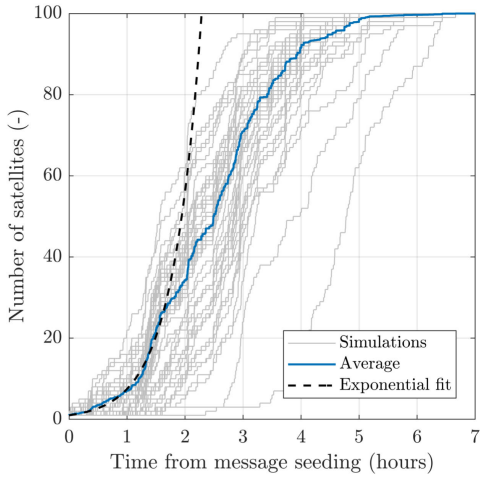

FIGURE 6. Single-frame message time to spread (TTS) results spectrum for the simulation 5. The results have been obtained via a Monte Carlo approach varying the satellite originally aware of the message at the beginning of the simulation. The time average of all the simulation realizations is shown in blue. An exponential fit to the message spreading initial portion is also shown.

The bidding process can be conducted following 3 different strategies, exploiting simple bidding mechanisms which, given the poor communicability of the network, aim at the minimization of the interactions among satellites:

1) Sequential bidding: in a sequential bidding scheme, the bidding phase starts when a consistent portion of the network ($> 95\%$) is aware that the task has been spread to all the network up to the spreading cutoff limit. The imaging window start must be delayed 12 hours to allow for the bidding process to complete. The chosen Earth observation federation is composed of 50 satellites in Sun Synchronous orbits concentrated around a local time of the ascending node LTAN $=$ 10.30 AM, and 50 satellites in near-polar (87 to 93 deg inclination) orbits. This is yielding an average TTS of 4 hours and 40 minutes. An imaging window starting 12 hours after the task seeding to the network allows the imaging task to be broadcasted and for the best-performing satellite reward function information to bid against the whole network, adding a 30% of extra time to allow for redundancy and worst-case scenarios.
2) Parallel bidding: in a parallel bidding scheme, the task spreading and the reward function bidding proceed simultaneously. Each satellite spreads the task along with its partial knowledge of the network cost functions up to date. Satellites stop bidding whenever their network reward function knowledge reaches the spreading cutoff limit. Both sequential and parallel

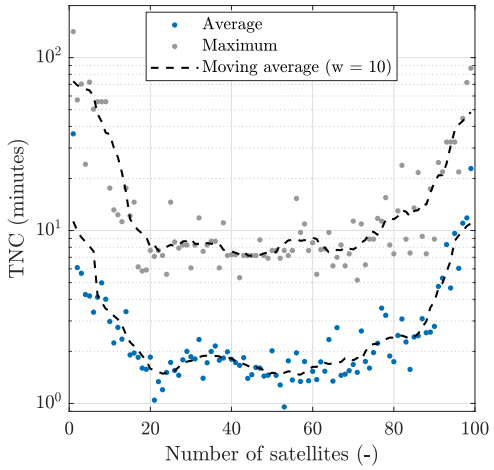

FIGURE 7. Maximum and average TNC results for the inter-satellite contact history pool originating from the conditions of simulation 5. An increased average TNC yields a diminished message spreading rate. High TNC maximum values yield a reduced robustness in the spreading process velocity.

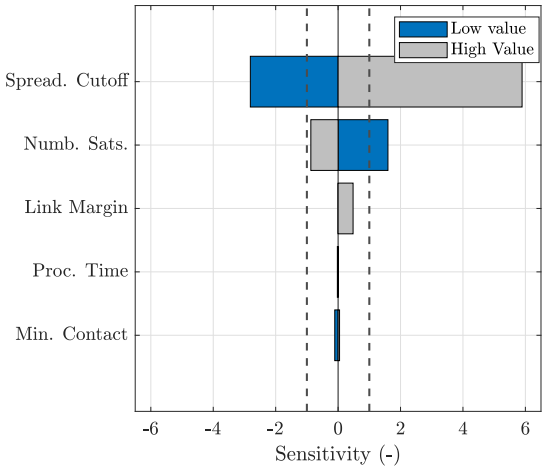

FIGURE 9. Tornado plot representing the single variable sensitivity analysis performed on the TTS metric. Sensitivities have been calculated as the ratio between the percentage variation in TTS with respect to the nominal case and the percentage variation of the input parameter with respect to the nominal one.

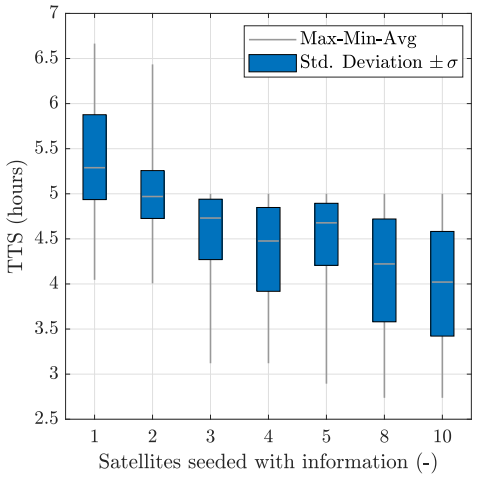

FIGURE 8. Multiseeding effect on simulation 5 conditions TTS results spectrum. Average, standard deviation, maximum and minimum values are shown.

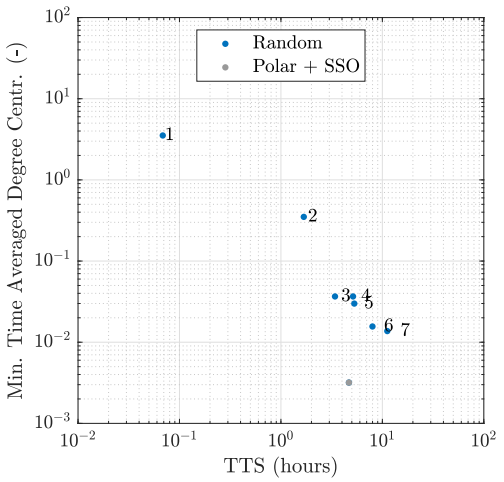

FIGURE 10. Least communicative satellite time-averaged degree centrality. Numbers associated to each data point represent the seven simulations IDs. The extra data point in grey represents the additional FSS orbital configuration employed for generality purposes.

bidding reward the highest function value regardless of the image acquisition timing. Regarding the imaging window boundaries, the same considerations for sequential bidding hold.

3) Reverse bidding: in a reverse auction, the auctioneer proposes a price and lowers it until one of the bidders accepts to buy. Compared to the two previous strategies, where the reward function value bid progressively increased, a reverse auction partly rewards bidding rapidity [30]. However, the absence of a centralized auctioneer and the poor communicability of the network require a modified approach. To reward early images, despite a generally higher cost in terms of satellite onboard resources, a time-evolving reward function is transmitted alongside the task. In this way, a monotone linear relation serves as a threshold where early images are traded against image quality. Any reward function value that overshoots the threshold is considered a feasible imaging opportunity, with no other need to communicate. For this reason, accurate tuning of the reward function time evolution is fundamental to avoid an excessive number of data products. An additional countermeasure to a disproportionate number of images involves sending a task spreading termination message whenever a single satellite reward function overshoots the threshold. The imaging window starts 3 hours after the imaging task seeding to the network, this is motivated by the absence of a proper bidding among satellites. With a reverse bidding scheme, it is in fact sufficient to let the task spread to a significant portion of the network.

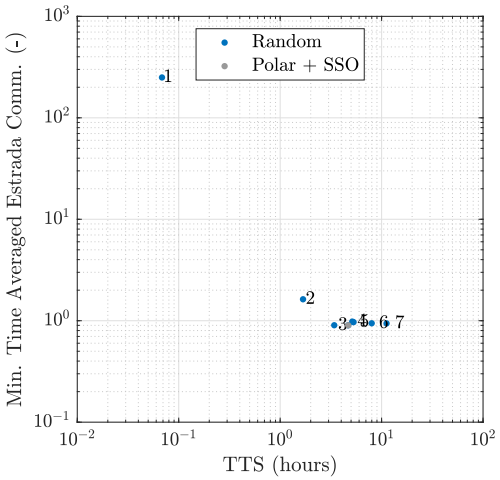

FIGURE 11. Least communicative satellite time-averaged Estrada communicability. Numbers associated to each data point represent the seven simulations IDs. The extra data point in grey represents the additional FSS orbital configuration employed for generality purposes.

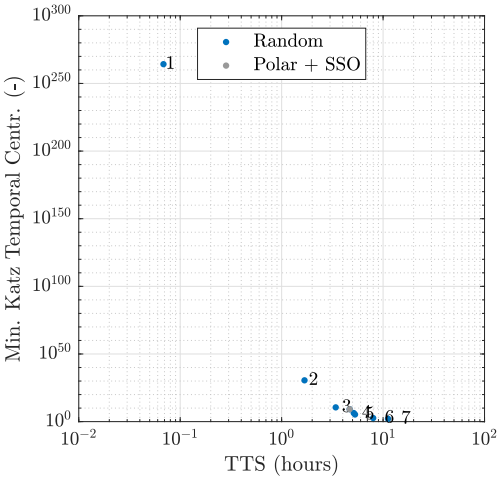

FIGURE 12. Least communicative satellite Katz dynamic centrality. Numbers associated with each data point represent the seven simulation IDs. The extra data point in grey represents the additional FSS orbital configuration employed for generality purposes.

The three strategies are applied to a specific use case, focused on the flooding event affecting the Italian region of Emilia-Romagna in May 2023. All the task details are presented in Table 5. The message size varies depending on the bidding strategy and the operative phase. The task for a 100-satellite federation can add up to 563 bytes (mainly occupied by the cloud coverage forecasting and the network update regarding the task spreading status) this message size remains almost constant for both sequential and parallel bidding strategies. Reverse bidding, which is not actively controlling the task spreading status in the network requires a task message size of only 261 bytes.

The results are analyzed in Sec.III in terms of network rapidity to reach global consensus over the chosen imager. From a theoretical point of view, the sequential bidding scheme requires the task message to be spread throughout the network once, and then the information regarding the reward function of the fittest satellite is required to be spread back to the whole network again. This process requires generally twice the TTS to reach global network consensus. In a parallel bidding scheme, the two pieces of information regarding the task and the best reward function spreading can be partially overlapped, thus requiring less than twice the TTS to reach global network consensus. Lastly, a reverse bidding approach requires only a single TTS to identify the fittest satellites for the observation. However, the number of satellites identified for the imaging campaign cannot be predetermined and depends solely on the chosen reward function time-varying threshold.

The results are presented by dividing the federation participants into three different categories:

1) Active: active federates are satellites whose reward function is temporarily the maximum of their own known subset of the network. At the end of the bidding

TABLE 5. Flooding event rapid mapping imaging task.

Parameter	Value	Unit
Federation participants	100	-
Task seeding time	03/05/2023 11.42 UTC	-
Image spectral window	380-700	nm
Imaging window start	03/05/2023 23.42 UTC	-
Imaging window end	04/05/2023 11.42 UTC	-
Target Latitude	44.28526389 N	deg
Target Longitude	11.88292222 E	deg
Ground Resolution	< 20	m

TABLE 6. Validation case dataset.

Parameter	Value	Unit
Satellite 1 altitude	500	km
Satellite 2 altitude	1000	km
Satellite 1 true anomaly	0	deg
Satellite 2 true anomaly	10	deg
Antenna gain (omnidirectional)	0	dBi
Coding Scheme	Reed Solomon (255,223)	-

TABLE 7. Simulations IDs and related hypotheses.

Sim. ID	Hypotheses	Notes
1	FP PP SX D10 C5 R100	Best-case scenario
2	FP SX D10 C5 R100	No mutual pointing
3	SX D10 C5 R100	RF transmission when power excess
4	HD D10 C5 R100	Half duplex communication
5	HD D10 C30 R100	30 seconds minimum contact
6	HD D10 C100 R100	100 seconds minimum contact
7	HD D10 C30 R50	Federation participants halved

TABLE 8. Sensitivity analysis input parameters.

Parameter	Low	Nominal	High
Spreading Cutoff	90%	95%	100%
Satellites Number	50	75	100
Link Margin	0 dB	3 dB	6 dB
On Board processing delay	5 s	10 s	15 s
Min. Continuous Contact	20 s	30 s	40 s

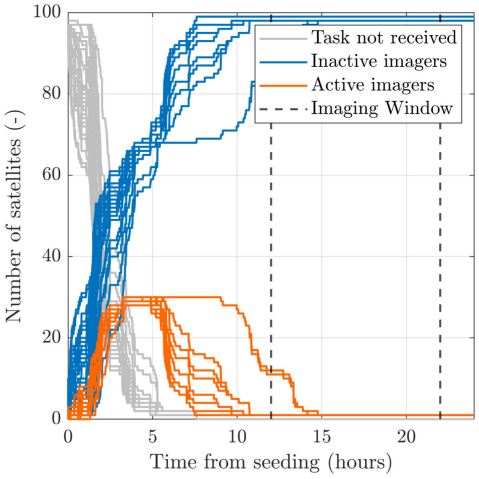

FIGURE 13. Sequential bidding FSS time response. Active, inactive, and uncontacted satellites' time evolutions are shown. An initial multiseeding operation to 3 satellites has been assumed. The imaging window is limited to 22 hours to leave up to 2 hours for image downlink to the ground segment.

window, active federates proceed to image the target location.

2) Inactive: inactive federates are satellites that cannot image the target location in the prescribed timeframe, as well as satellites that have already lost the bidding process with an active federate.
3) Uncontacted: uncontacted federates are satellites that still have to be reached by the imaging task.

Fig. 13 and Fig. 14 show the results of the disaster response monitoring use case when employing a sequential bidding strategy. In some simulations, the sequential bidding approach can only reach a total network consensus after the beginning of the observation window. This is due to the lag introduced by the separation of spreading and bidding phases. As shown in Fig.13, inactive imagers are characterized by a two-step growth. At first, satellites auto-exclude observation when no imaging opportunity is computed onboard. Subsequently, the bidding process forces satellites to transition from active to inactive. However, if the task spreading interrupts temporarily, the transition to the bidding phase is postponed, and therefore, a large number of satellites are activated for the observation, characterized by several sub-optimal images produced in a restricted time window. The imaging opportunity, in common with parallel bidding, is characterized by a Sun elevation on target of 18 deg and a cloud coverage of 30%. The target imaging implies an 8.8-degree deviation from the nominal Nadir pointing attitude. Fig. 15 and Fig. 16 show the results regarding the parallel bidding strategy. This bidding scheme is revealed to be faster than sequential bidding, always reaching a total network consensus on the active satellite within the imaging window earliest bound. Another advantage of such a bidding strategy is the continuous deactivation of most non-optimal imagers. This strategy results in increased robustness, keeping the number of active imagers constantly below ten units, minimizing the number of images. This minimization fosters the least waste of the federation's resources. In addition, a smaller number of active imagers reduces the range of reward function values available to the network in the case of delayed spreading. Fig. 17 presents the results for the reverse bidding scheme, considering the time-varying reward function rise as in Fig. 18. Such a threshold enforces a linear trade-off between image rapidity and quality. The choice of the initial value is motivated by the minimum value that could be reached by the reward function given the thresholds on onboard resources and image quality in place. Reverse bidding provides a faster alternative, allowing for a larger imaging window. In this specific case, the reward function time evolution tuning allows to effectively select only one satellite in the simulation. However, this also results in the most significant drawback of the strategy itself. The high dependency of the outcome with respect to the reward function evolution in time may result in more than a single active imager, wasting the federation's resources, depending on the specific federation configuration. However, an extension of the observation window allows for the generation of extremely rapid data products and expands the observation chances in the 24-hour time frame required by disaster response monitoring. Specifically, extending the imaging time window allows more reliable rapid mapping capabilities even with a reduced daylight duration on the target (targets at high latitudes in the winter season). The imaging opportunity provided is comparable to the one presented by sequential and parallel bidding in terms of the reward function value, with a Sun elevation on target equal to 12 deg, a cloud coverage of 24%, and a required slew from the camera nominal nadir pointing attitude of 23.8 deg. An overall comparison of the three strategies is presented in Table 9. From a global perspective, sequential bidding, provides a reliable solution. However the sequential bidding was observed to be excessively slow in reaching network consensus, clogging the network for an unnecessarily long period of time. Parallel bidding emerges as a moderately fast and reward function near-optimal solution. Reverse bidding is the fastest strategy. However it strongly depends on the choice of the reward function threshold, which can potentially lead to a waste of resources for the network.

IV. FUTURE WORK AND CONCLUSION

A. FUTURE WORK

Although the present work strives to give a complete perspective of the issue, possible extensions and ulterior developments should be addressed in the following directions. A more comprehensive simulator with fully functional hardware in the loop capabilities should be developed, allowing for space-rated hardware to be connected to the simulation in order to provide a fully functional test bench for full-stack FSS communication protocols. In addition,

TABLE 9. Bidding strategies observation opportunities comparison.

Bidding strategy	Imaging Sat. ID	Observation Time [CEST]	Reward J	J_{Sun} [0-1]	J_{Cloud} [0-1]	J_{ADCS} [0-1]	$J_{Battery}$ [0-1]
Sequential	37	04/05/2023 07.53.27	0.663	0.308	0.700	0.951	1
Parallel	37	04/05/2023 07.53.27	0.663	0.308	0.700	0.951	1
Reverse	81	03/05/2023 18.57.31	0.639	0.205	0.761	0.868	1

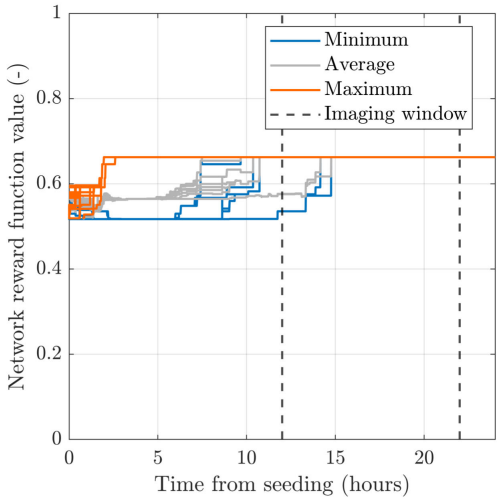

FIGURE 14. Sequential bidding reward function time evolution. Maximum, average and minimum reward function values are shown.

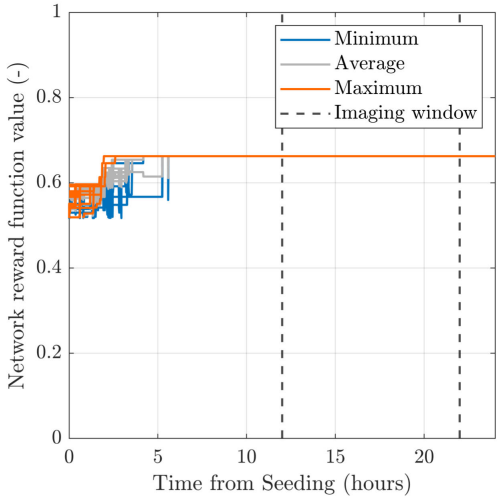

FIGURE 16. Parallel bidding reward function time evolution. Maximum, average, and minimum reward function values are shown.

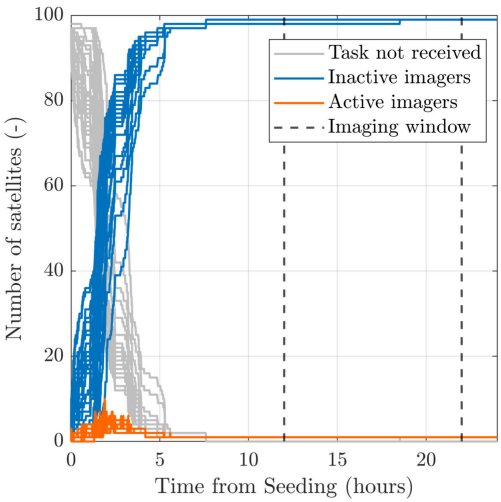

FIGURE 15. Parallel bidding FSS time response. Active, inactive, and uncontacted satellites' time evolutions are shown. An initial multiseeding operation to 3 satellites has been assumed. The imaging window is limited to 22 hours to leave up to 2 hours for image downlink to the ground segment.

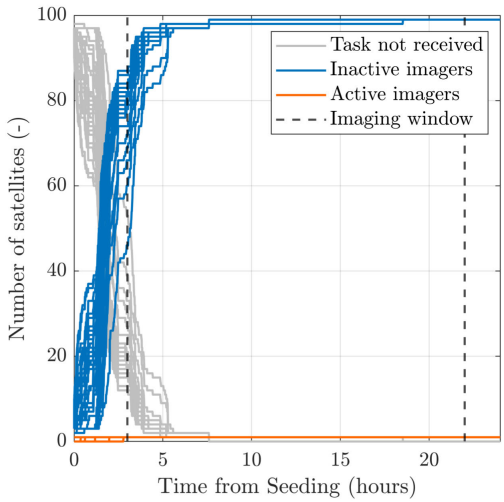

FIGURE 17. Reverse bidding FSS time response. Active, inactive, and uncontacted satellites' time evolutions are shown. An initial multiseeding operation to 3 satellites has been assumed. The imaging window is limited to 22 hours to leave up to 2 hours for image downlink to the ground segment.

a more comprehensive network simulation dataset should be produced, increasing the current number of verified hypotheses and providing a more robust basis on which the communicability metrics evidence can be confirmed. The network bridging effect of ground stations in the task spreading process should be investigated as well, especially in light of the heterogeneous frequency bands usually employed by different satellite platforms, which can potentially create subnetworks that are hardly linkable between each other in other ways. Moreover, a more structured approach to the bidding algorithms should be developed, adapting to the poor communicability of the satellite network novel bidding mechanisms, characterized by a more explicit optimality metric for the autonomous scheduling problem.

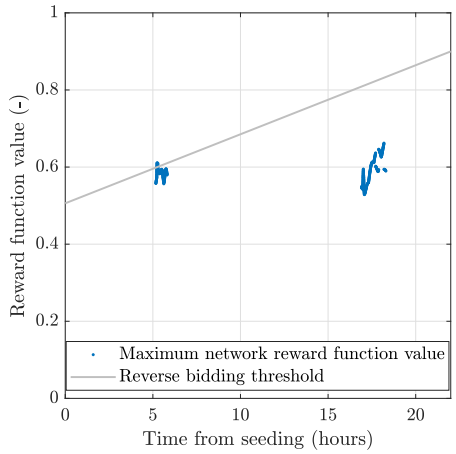

FIGURE 18. Reverse bidding reward function threshold versus maximum reward function values per each satellite in the federation.

B. CONCLUSION

The present work concentrates on the development of a simulation infrastructure to allow for better physical layer modeling in federated satellite systems inter-satellite communication, proving the capability of a FSS to effectively sustain networked operations. The development of the simulator takes advantage of the IEEE 1516.2010 high-level architecture standard, allowing for functional verification of potential hardware in the loop capabilities. The simulator propagates a one hundred 6U CubeSat federation capable of constituting a satellite FSS network exploiting UHF inter-satellite links. Specifically, network communicability has been tested under several onboard resources and operative constraints to highlight the reduced network capabilities both in terms of message spreading and data volume exchange. The average time needed to spread a single-frame message to the whole network, accounting for 30 seconds of half duplex, uninterrupted contact, is over 5 hours in the case of a superimposition of FSS operations over nominal satellite operations, with a mean time-averaged goodput of 2.6 bps per inter-satellite connection. Despite poor communicability greatly affects the capabilities of the FSS network to negotiate services and tasks, a disaster response monitoring use case has been analyzed, assessing the FSS network's capability to sustain an autonomous target observation scheduling task in a time-critical scenario. The results prove that an online auction-based autonomous scheduling bidding strategy, parallelizing both the imaging task spreading and the scheduling bidding, is still capable of providing a sufficiently fast response to a rapid mapping request following a natural disaster. The federation is, in fact, capable of consistently reaching a task allocation global consensus on a single satellite imager in under 8 hours, succeeding in proving the applicability of the FSS to time-critical scenarios.

ACKNOWLEDGMENT

The authors thank Professor Francesco Topputo (Politecnico di Milano) for making the research exchange that led to the development of this article possible.

REFERENCES

[1] D. Selva, A. Golkar, O. Korobova, I. L. I. Cruz, P. Collopy, and O. L. de Weck, "Distributed earth satellite systems: What is needed to move forward?" *J. Aerosp. Inf. Syst.*, vol. 14, no. 8, pp. 412–438, 2017.

[2] M. Safyan, *Planet's Dove Satellite Constellation*. Cham, Switzerland: Springer, 2020, pp. 1–17.

[3] N. Pachler, I. del Portillo, E. F. Crawley, and B. G. Cameron, "An updated comparison of four low Earth orbit satellite constellation systems to provide global broadband," in *Proc. IEEE Int. Conf. Commun. Workshops (ICC Workshops)*, Jun. 2021, pp. 1–7.

[4] D. Muff, V. Ignatenko, O. Dogan, L. Lamentowski, P. Leprovost, M. Nottingham, A. Radius, T. Seilonen, and V. Tolpekin, "The ICEYE constellation–some new achievements," in *Proc. IEEE Radar Conf. (RadarConf)*, Mar. 2022, pp. 1–4.

[5] A. Golkar and I. L. I. Cruz, "The federated satellite systems paradigm: Concept and business case evaluation," *Acta Astronautica*, vol. 111, pp. 230–248, Jun. 2015.

[6] D. Rashkovetsky, F. Mauracher, M. Langer, and M. Schmitt, "Wildfire detection from multisensor satellite imagery using deep semantic segmentation," *IEEE J. Sel. Topics Appl. Earth Observ. Remote Sens.*, vol. 14, pp. 7001–7016, 2021.

[7] J. A. Ruiz de Azúa, A. Calveras, and A. Camps, "Internet of satellites (IoSat): Analysis of network models and routing protocol requirements," *IEEE Access*, vol. 6, pp. 20390–20411, 2018.

[8] J. A. Ruiz-De-Azua, A. Calveras, and A. Camps, "A novel dissemination protocol to deploy opportunistic services in federated satellite systems," *IEEE Access*, vol. 8, pp. 142348–142365, 2020.

[9] I. Lluch, P. T. Grogan, U. Pica, and A. Golkar, "Simulating a proactive ad-hoc network protocol for federated satellite systems," in *Proc. IEEE Aerosp. Conf.*, Mar. 2015, pp. 1–16.

[10] O. von Maurich and A. Golkar, "Data authentication, integrity and confidentiality mechanisms for federated satellite systems," *Acta Astronautica*, vol. 149, pp. 61–76, Aug. 2018.

[11] R. Alena, Y. Nakamura, N. Faber, and D. Mauro, "Heterogeneous spacecraft networks: Wireless network technology assessment," in *Proc. IEEE Aerosp. Conf.* Union City, NJ, USA: Wire, Mar. 2014, pp. 1–13.

[12] A. Z. M. Shahriar, M. Atiquzzaman, W. D. Ivancic, and L. Wood, "A sender-based TFRC for Saratoga: A rate control mechanism for a space-friendly transfer protocol," in *Proc. Aerosp. Conf.*, Mar. 2011, pp. 1–12.

[13] L. Xiangqun, W. Lu, L. Lixiang, H. Xiaohui, X. Fanjiang, and C. Jing, "OMNeT++ and mixim-based protocol simulator for satellite network," in *Proc. Aerosp. Conf.*, Mar. 2011, pp. 1–9.

[14] P. Muri, J. McNair, J. Antoon, A. Gordon-Ross, K. Cason, and N. Fitz-Coy, "Topology design and performance analysis for networked Earth observing small satellites," in *Proc. MILCOM Mil. Commun. Conf.*, Nov. 2011, pp. 1940–1945.

[15] B. Barritt, K. Bhasin, W. Eddy, and S. Matthews, "Unified approach to modeling & simulation of space communication networks and systems," in *Proc. IEEE Int. Syst. Conf.*, Apr. 2010, pp. 133–136.

[16] J. A. Ruiz-de-Azúa, C. Araguz, A. Calveras, E. Alarcón, and A. Camps, "Towards an integral model-based simulator for autonomous Earth observation satellite networks," in *Proc. IEEE Int. Geosci. Remote Sens. Symp.*, Jul. 2018, pp. 7403–7406.

[17] Jeroen Cappaert and Sreeja Nag, "Network control systems for large-scale constellations," in *Handbook of Small Satellites*. Cham, Switzerland: Springer, 2020.

[18] Y. Liu, Q. Chen, C. Li, and F. Wang, "Mission planning for Earth observation satellite with competitive learning strategy," *Aerosp. Sci. Technol.*, vol. 118, Nov. 2021, Art. no. 107047.

[19] P. T. Grogan, "Modeling challenges for Earth observing systems of systems," in *Proc. IEEE Int. Geosci. Remote Sens. Symp.*, Jul. 2019, pp. 5289–5292.

[20] *IEEE Standard for Modeling and Simulation (M&S) High Level Architecture (HLA)—Framework and Rules*, Standard 1516-2010 (Revision of IEEE Std 1516-2000), 2010, pp. 1–38.

[21] M. Gütlein, W. Baron, C. Renner, and A. Djanatliev, "Performance evaluation of HLA RTI implementations," in *Proc. IEEE/ACM 24th Int. Symp. Distrib. Simulation Real Time Appl. (DS-RT)*, Sep. 2020, pp. 1–8.

[22] J.-B. Chaudron, M. Adelantado, E. Noulard, and P. Siron, "Hla high performance and real-time simulation studies with certi," in *Proc. 25th Eur. Simul. Model. Conf. (ESM)*, Guimaraes, Portugal, Oct. 2011.

[23] A. Camps, A. Golkar, A. Gutierrez, J. Ruiz-de Azua, J. Munoz-Martin, L. Fernandez, C. Diez, A. Aguilella, S. Briatore, R. Akhtyamov, and N. Garzaniti, "Fsscat, the 2017 Copernicus masters' 'Esa sentinel small satellite challenge' winner: A federated polar and soil moisture tandem mission based on 6u cubesats," in *Proc. IEEE Int. Geosci. Remote Sens. Symp.*, Jul. 2018, pp. 8285–8287.
[24] E. Estrada and D. J. Higham, "Network properties revealed through matrix functions," *SIAM Rev.*, vol. 52, no. 4, pp. 696–714, Jan. 2010.
[25] E. Estrada and N. Hatano, "Communicability in complex networks," *Phys. Rev. E, Stat. Phys. Plasmas Fluids Relat. Interdiscip. Top.*, vol. 77, no. 3, Mar. 2008, Art. no. 036111.
[26] P. Grindrod, M. C. Parsons, D. J. Higham, and E. Estrada, "Communicability across evolving networks," *Phys. Rev. E, Stat. Phys. Plasmas Fluids Relat. Interdiscip. Top.*, vol. 83, no. 4, Apr. 2011, Art. no. 046120.
[27] K. Schilling and M. Schmidt, "Communication in distributed satellite systems," in *Distributed Space Missions for Earth System Monitoring*. New York, NY, USA: Springer, 2013, pp. 345–354.
[28] P. Bonacich, "Power and centrality: A family of measures," *Amer. J. Sociol.*, vol. 92, no. 5, pp. 1170–1182, Mar. 1987.
[29] Q. Yang, B. Song, Y. Chen, L. He, and P. Wang, "A distributed autonomous mission planning method for the low-orbit imaging constellation," *Algorithms*, vol. 16, no. 10, p. 475, Oct. 2023.
[30] U. Pica and A. Golkar, "Sealed-bid reverse auction pricing mechanisms for federated satellite systems: Sealed-bid reverse auction pricing mechanisms," *Syst. Eng.*, vol. 20, no. 5, pp. 432–446, 2017.

SIMONE SCROCCIOLANI received the B.S. and M.S. degrees in space engineering from Politecnico di Milano, Italy, in 2021 and 2023, respectively.

In 2023, he participated in a research exchange with the Chair of Pico and Nano Satellites and Satellite Constellations, Technische Universität München. His main research interests include systems engineering applied to satellite communications and space electro-optical payloads for earth observation.

VINCENZO MESSINA received the master's degree in space engineering from Politecnico di Milano. He is currently pursuing the Ph.D. degree with Technische Universität München.

He was a Researcher with the University of Southampton, focusing on on-board propulsion systems. In 2022, he started his doctoral program on the development of new algorithms and methods for optimizing the operations and coordination of a federation of satellites in a decentralized manner, where each satellite operates autonomously and independently while still achieving a collective goal.

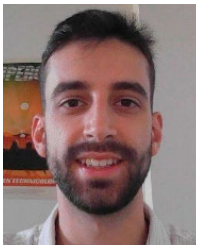

RAMÓN MARÍA GARCÍA ALARCIA received the master's degree in aerospace engineering from ISAE-SUPAERO, specializing in space systems. He is currently pursuing the Ph.D. degree with Technische Universität München.

In 2022, he started his doctoral program on the application of generative AI technology to the design of space missions, focusing on building a design assistant tool to facilitate and streamline the initial phases of spacecraft design.

JASPAR SINDERMANN received the bachelor's degree in mechanical engineering from Universität Kassel and the master's degree in aerospace engineering from Technische Universität München, where he is currently pursuing the Ph.D. degree.

In 2022, he started his doctoral program in the framework of model-based systems engineering, specializing in the development of a modular distributed simulator for space systems.

ALESSANDRO GOLKAR received the B.Sc. and M.Sc. degrees in aerospace engineering from the University of Rome "La Sapienza," and the Ph.D. degree in aeronautics and astronautics from the Massachusetts Institute of Technology (MIT).

He is currently a Professor with Technische Universität München and the Chair of Pico-, Nanosatellites, and Satellite Constellations. From 2012 to 2022, he was among the founding faculty members of the Skolkovo Institute of Science and Technology (Skoltech), a new research university founded in collaboration with MIT. From 2017 to 2019, he took a sabbatical leave from academia and joined Airbus as the Vice President Concurrent Engineering of the Technology Planning and Roadmapping Unit, Corporate Technology Office. His research interests include systems engineering and in the development of novel mission concepts of spacecraft systems, with particular interest in nanosatellites and satellite constellation systems.

Dr. Golkar serves as an Associate Editor for *INCOSE Systems Engineering* journal.